On the Performance of RSMA-Based Visible Light Communication Systems With Multicolor LED

Manh Le-Tran and Thai-Hoc Vu, *Member, IEEE*

***Abstract*—In this work, we analyze the performance of rate-splitting multiple access (RSMA) in visible light communication (VLC) systems using multicolor light-emitting diodes (LEDs). The system splits the data of users into a common stream decoded by all users and user-specific private streams, maps these streams onto the color channels of a multicolor LED, and uses successive interference cancellation (SIC) at the receiver side to exploit color diversity. Closed-form expressions are derived for the key performance metrics such as outage probability (OP), coverage probability, and ergodic sum rate under the Lambertian channel model. To concurrently mitigate multiuser interference, which arises from cross-color coupling, and optimize the power division between the common and private data streams, a joint precoding and power allocation strategy is implemented. More specifically, the resulting nonconvex optimization problem is efficiently solved by an equivalent convex reformulation to efficiently obtain the optimal power allocation coefficients. Numerical results demonstrate that in the low-to-moderate common rate regime, RSMA demonstrates superior performance over the conventional scheme regarding coverage probability and ergodic sum rate. This improvement further enhances the reliability and spectral efficiency for VLC systems that employ practical multicolor LED configurations.**

***Index Terms*—Multicolor light-emitting diode (LED), outage probability (OP), rate-splitting multiple access (RSMA), visible light communication (VLC).**

I. Introduction

THE growing demand for high-capacity wireless services, such as augmented reality and high-definition video streaming, necessitates exploring new spectrum resources beyond conventional radio frequency (RF) techniques. Visible light communication (VLC), operating in the unlicensed optical band, is a promising solution due to its abundant bandwidth, high security, and immunity to RF interference [1], [2]. Indoor VLC systems using white light-emitting diodes (LEDs) offer the dual purpose of lighting and communication, but their performance is often limited by multipath reflections and multiuser interference [3], [4]. While techniques like angle-diversity receivers [5] and deep learning-based optimization [6] have improved capacity and robustness, the inherent multiuser interference in dynamic indoor cells remains a bottleneck for network throughput and reliability.

Given the difficulties inherent in the system, rate-splitting multiple access (RSMA) stands out as a high-performance framework for multiuser downlink communication [7]. Specifically, RSMA splits the message of each user into a common part, which is decoded by all users, and a private part, which is decoded only by the intended recipient, then utilizes successive interference cancellation (SIC) at the receiver. This allows for a flexible interference management, generalizing and unifying conventional schemes like orthogonal multiple access (OMA) and non-OMA (NOMA) [8]. Consequently, RSMA offers significant improvements in spectral and energy efficiency over existing schemes. However, the research on RSMA-enabled VLC systems is relatively limited. Most existing VLC research relies on simpler techniques [9], [10], which struggle with complex multiuser interference and dynamic user distributions. Recent results confirm that RSMA significantly outperforms conventional techniques in indoor VLC channels by superiorly handling multiuser interference [11] while careful design of RSMA parameters can significantly improve overall system performance [12]. This clear advantage establishes RSMA as an important area for research to maximize the capacity of VLC deployments.

Moreover, multicolor LED systems, such as red, green, blue, and yellow (RGBY) ones, offer the ability to achieve parallel data transmission over different wavelengths, further boosting spectral efficiency and supporting multiuser access [13]. While the multicolor VLC architecture brings new opportunities, it also introduces unique challenges. Recent receiver design principles with quadrichromatic LEDs demonstrate that optimized photodiode (PD) orientation can improve bit error rate (BER) performance compared with conventional designs [14]. In addition, energy-efficient power allocation strategies for multicolor VLC systems have been shown to reduce consumption while meeting illumination and signal-to-interference-plus-noise ratio (SINR) constraints [15]. Naser et al. [16] consider RSMA in a white-LED VLC setting without color-domain mixing, providing an overview and a two-user simulation that shows sum-rate gains over NOMA. Also, prior works [11], [12], [16] focus on algorithmic or numerical evaluations of the RSMA system and do not include performance analysis based on statistical channel

Received 26 October 2025; revised 20 November 2025; accepted 24 November 2025. Date of publication 26 November 2025; date of current version 5 February 2026. This work was supported by the Ministry of Education, Youth and Sports of Czech Republic (MEYS CZ) through the Student Grant Competition in the VSB-Technical University of Ostrava under Project SGS SP2025/013. *(Corresponding author: Manh Le-Tran.)*

Manh Le-Tran is with the Faculty of Electronics and Telecommunications, VNU University of Engineering and Technology, Hanoi 123106, Vietnam (e-mail: manhlt@vnu.edu.vn).

Thai-Hoc Vu is with the Faculty of Electrical Engineering and Computer Science, VSB-Technical University of Ostrava, 708 00 Ostrava, Czechia (e-mail: thai.hoc.vu@vsb.cz).

Digital Object Identifier 10.1109/JIOT.2025.3637758

2327-4662 © 2025 IEEE. All rights reserved, including rights for text and data mining, and training of artificial intelligence and similar technologies. Personal use is permitted, but republication/redistribution requires IEEE permission.
See https://www.ieee.org/publications/rights/index.html for more information.

Authorized licensed use limited to: Technical University of Ostrava. Downloaded on March 03,2026 at 20:56:13 UTC from IEEE Xplore. Restrictions apply.

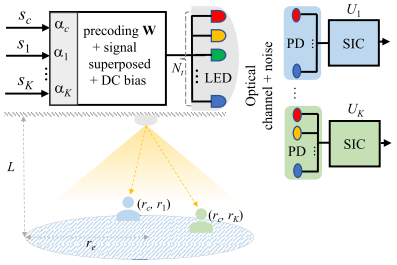

Fig. 1. Model of proposed system.

gains. Furthermore, the multicolor structure can facilitate the deployment of RSMA, where the common and private parts can be split across colors, and per-color power can be allocated to balance interference and illumination constraints. However, wavelength-dependent channel, intensity-modulation and direct-detection (IM/DD) constraints, and cross-color interference complicate the design of precoder and power allocation strategies [17].

To the best of our knowledge, prior RSMA works in the literature assume white-LED channels without color mixing, and no prior article has developed an RSMA framework for multicolor-LED VLC. There is a need for rigorous analytical frameworks for multicolor-LED-based systems that provide closed-form expressions for outage probability (OP), coverage probability, and ergodic sum rate under channels with IM/DD constraints and significant cross-color interference. Furthermore, there is a limited analysis concerning the joint impact of per-color power allocation, RSMA common/private stream splitting, and the effects of LED semiangle and user location. This framework enables a direct comparison with conventional schemes under the same assumptions. The main contributions of this article are summarized as follows.

1) We propose a multicolor VLC system employing RSMA to perform color-domain rate-splitting by mapping the common and private streams across the channels with per-color power shares while satisfying lightning and IM/DD limits, thereby exploiting color diversity to manage interference without compromising illumination.
2) A joint precoding and power allocation scheme is considered to exploit color diversity and effectively mitigate multiuser interference.
3) Derive closed-form expressions for OP, coverage probability, and ergodic sum rate for uniformly distributed indoor users under a wavelength-dependent crosstalk matrix and Lambertian model.
4) Through simulations, we validate the analytical results and demonstrate that RSMA outperforms NOMA, OMA, and white-LED based RSMA under moderate common-power allocation. We also analyze the impact of key parameters on the system performance.

II. Proposed RSMA-Based Scheme

A. System Model and SINR Statistic

For the indoor VLC system with IM/DD in Fig. 1, a multicolor LED with N_t chips is employed to convey the information to K users $U_k, k \in \{1, 2, \ldots, K\}$. More specifically, we consider the transmitter is mounted on the ceiling, and user locations follow a uniform distribution over a disk-shaped area. The vertical distance between the LED and the receiving plane is L. The maximum cell radius is r_e while only line-of-sight (LOS) VLC links are taken into account [18]. Furthermore, it is assumed that the kth user is equipped with N_k PDs, where each PD operates at a wavelength corresponding to one chip among N_t chips of LED sources S.

To improve the overall spectral efficiency of the system when multiple users are served simultaneously, S employs RSMA by partitioning the intended messages of users into common and private parts. At the transmitter side, all common parts are aggregated into the common stream s_c, whereas the private portions are mapped to the private streams s_k through power-domain multiplexing. These streams are subsequently scaled with their associated precoding coefficients and then conveyed via light intensity. At the receiver side, SIC is employed by each user to decode the common stream before retrieving the private streams. The transmitted signal at $\mathcal{S}$ based on the RSMA principle can be expressed as

$$\mathbf{x} = \sqrt{\alpha_c}\sqrt{P_e}\mathbf{w}_c s_c + \sum_{k=1}^{K}\sqrt{\alpha_k}\sqrt{P_e}\mathbf{w}_k s_k + \mathbf{J}_{\mathrm{dc}} \quad (1)$$

where $\mathbf{w}_c \in \mathbb{R}^{N_t \times 1}$ and $\mathbf{w}_k \in \mathbb{R}^{N_t \times 1}$ are the precoding weights for s_c and s_k. Also, the allocated electrical power for the information signals is denoted as P_e and the direct current (dc) bias vector $\mathbf{J}_{\mathrm{dc}}$ applied across the LEDs to maintain the lightning constraint. Moreover, α_c and α_k denote the power allocation coefficients of s_c and s_k, respectively. The constraint on total power requires that the power allocation coefficients satisfy the following condition

$$\alpha_c + \sum_{k=1}^{K}\alpha_k = 1. \quad (2)$$

In the considered model, each user is assumed to be equipped with a distinct number of PDs, with every PD corresponding to a specific color emitted by the multicolor LED. Let $\mathbf{I}_k$ denote a $1 \times N_t$ vector that characterizes the PD arrangement of the kth user. In particular, when the nth entry of $\mathbf{I}_k$ equals one, it indicates that the kth user employs a PD whose wavelength property matches that of the nth LED chip. This assumption also reflects practical receiver design, since assigning each PD to a specific wavelength not only reduces hardware complexity and cost, but also mitigates cross-color interference if a single PD were exposed to multiple LED chips simultaneously. The optical transmit power from each LED can be expressed as

$$P_o = \alpha\mathbb{E}[x] = \eta\mathbf{J}_{\mathrm{dc}}. \quad (3)$$

In here, η is the conversion efficiency of the LED, and we set $\eta = 1$ without loss of generality. Accordingly, at U_k, the received signal transmitted through the channel matrix $\mathbf{H}_k$, after removing the dc bias, can be expressed as

$$\mathbf{y}_k = \mathbf{I}_k\mathbf{H}_k\left(\sqrt{\alpha_c}\sqrt{P_e}\mathbf{w}_c x_c + \sum_{k=1}^{K}\sqrt{\alpha_k}\sqrt{P_e}\mathbf{w}_k x_k\right) + \mathbf{n}_k \quad (4)$$

Authorized licensed use limited to: Technical University of Ostrava. Downloaded on March 03,2026 at 20:56:13 UTC from IEEE Xplore. Restrictions apply.

where $\mathbf{n}_k$ denotes the noise vector in which every entry follows $\mathcal{CN}(0,\sigma^2)$, representing the additive white Gaussian noise, whereas the remaining components take zero values.

Following the approach in [14], the channel matrix $\mathbf{H}_k$ is modeled as $\mathbf{H}_k = h_k\mathbf{V}$, where $\mathbf{V} \in N_t \times N_t$ acts as the crosstalk matrix. Within a single-layer SIC receiver, the SINRs at U_k for decoding x_c and x_k can be written as

$$\gamma_c^k = \frac{\alpha_c \rho h_k^2 \left|\mathbf{q}_k \mathbf{w}_c\right|^2}{\alpha_k \rho h_k^2 \left|\mathbf{q}_k \mathbf{w}_c\right|^2 + \sum_{j=j\neq k}^{K} \alpha_j \rho h_k^2 \left|\mathbf{q}_k \mathbf{w}_j\right|^2 + 1} \tag{5}$$

$$\gamma_p^k = \frac{\alpha_k \rho h_k^2 \left|\mathbf{q}_k \mathbf{w}_k\right|^2}{\sum_{j=1,j\neq k}^{K} \alpha_j \rho h_k^2 \left|\mathbf{q}_k \mathbf{w}_j\right|^2 + \alpha_c \rho h_k^2 \left|\mathbf{q}_k \mathbf{w}_c\right|^2 + 1} \tag{6}$$

where $\mathbf{q}_k = \mathbf{I}_k\mathbf{V}$ and $\rho = P_e/\sigma^2$ are the transmit signal-to-noise ratios (SNRs).

We have γ_c^k and γ_p^k, which are maximized when $\mathbf{q}_k$ is aligned with $\mathbf{w}_c$ and $\mathbf{w}_k$. Multiuser interference is eliminated if $\mathbf{q}_k$ is orthogonal to $\mathbf{w}_j$, as $\mathbf{q}_k\mathbf{w}_j = 0$, thereby $\mathbf{q}_k\mathbf{w}_c = \|\mathbf{q}_k\|$ and $\mathbf{q}_k\mathbf{w}_k = \|\mathbf{q}_k\|$. For the private precoding weights, zero forcing (ZF) and maximum ratio transmission (MRT) [19] are considered to obtain $\mathbf{q}_k\mathbf{w}_j = 0$ and $\mathbf{q}_k\mathbf{w}_k = \|\mathbf{q}_k\|$. This can be done by letting $\mathbf{W} = \mathbf{Q}(\mathbf{Q}^\dagger\mathbf{Q})^{-1}\mathbf{U} = [\mathbf{w}_1, \ldots \mathbf{w}_K] \in \mathbb{C}^{N_t \times K}$, where $\mathbf{Q} = [\mathbf{q}_1^T, \ldots \mathbf{q}_K^T]$ and $\mathbf{U} = \text{diag}(\|\mathbf{q}_k\|, \ldots, \|\mathbf{q}_k\|, \ldots, \|\mathbf{q}_k\|)$.

Furthermore, to ensure $\mathbf{q}_k\mathbf{w}_c = \|\mathbf{q}_k\|$ for all k, we exploit the ZF structure $\mathbf{q}_k\mathbf{w}_j = 0$ for $j \neq k$ together with the precoder matrix $\mathbf{W} = [\mathbf{w}_1, \ldots, \mathbf{w}_K]$. Let $\mathbf{I}$ denote the K-dimensional all-ones vector. Choosing $\mathbf{w}_c = \mathbf{WI} \in \mathbb{C}^{N_t \times 1}$ could meet the requirement, since $\mathbf{WI} = \sum_{k=1}^{K} \mathbf{w}_k$. Hence, the common precoder equals the sum of the private precoders. Then, the kth column of $\mathbf{W}$ is the private precoder for stream x_k. From the above principle, (5) and (6) become

$$\gamma_c^k = \frac{\alpha_c h_k^2 \beta_k}{\alpha_k h_k^2 \beta_k + 1}, \gamma_p^k = \frac{\alpha_k h_k^2 \beta_k}{\alpha_c h_k^2 \beta_k + 1} \tag{7}$$

where $\beta_k = \rho\|\mathbf{q}_k\|^2$. The achievable rate for the kth user is

$$R^k = R_c^k + R_p^k = \frac{1}{2}\log_2\left(1 + \gamma_c^k\right) + \frac{1}{2}\log_2\left(1 + \gamma_p^k\right). \tag{8}$$

B. Channel Statistic

Let $\phi_{1/2}$ denotes the LED semiangle at half power and $m = -\ln(2)/\ln(\cos\phi_{1/2})$ be the Lambertian order. For U_k, A_k and Q_k are the detection area and responsivity of PD, respectively. ψ_k is the incidence angle, and Ψ_c is the PD field of view (FOV). The optical filter and concentrator have gains $U(\psi_k)$ and $g(\psi_k)$, respectively. We define the constant

$$C = \frac{U(\psi_k)\, g(\psi_k)\, A_k\, Q_k}{2\pi} \tag{9}$$

so the channel gain from the LED sources to the PDs of the kth user can be expressed as [20]

$$h_k = C\,(m+1)\,\frac{L^{m+1}}{\left(r_k^2 + L^2\right)^{\frac{m+3}{2}}}. \tag{10}$$

As a result, the probability density function (pdf) of h_k^2 is

$$f_{h_k^2}(t) = -\xi_0 t^{-\frac{1}{m+3}-1} \tag{11}$$

where $\xi_0 = -(1)/(r_e^2)(1)/(m+3)(C(m+1)L^{m+1})^{(2)/(m+3)}$. We also have $t \in [\xi_{\min}, \xi_{\max}]$, where $\xi_{\min}$ and $\xi_{\max}$ are given as $\xi_{\min} = (C(m+1)L^{m+1})^2/(r_e^2 + L^2)^{m+3}$ and $\xi_{\max} = (C(m+1)L^{m+1})^2/L^{2(m+3)}$. Integrating (11) over $[\xi_{\min}, \xi_{\max}]$, the cumulative distribution function (cdf) of the variable h_k^2 can therefore be obtained as

$$F_{h_k^2}(t) = \xi_0 t^{-\frac{1}{m+3}} + \frac{L^2}{r_e^2} + 1. \tag{12}$$

Since $f_{h_k^2}(t) > 0$, $F_{h_k^2}(t)$ is strictly increasing on $(\xi_{\min}, \xi_{\max})$. Hence, for any thresholds θ_k within this interval, minimizing $P_k^{\text{out}} = F_{h_k^2}(\theta_k)$ is equivalent to minimizing θ_k.

III. Performance Analysis

In this section, we investigate the relationship between various parameters and performance metrics to provide deeper insight into the impact of channel conditions on performance.

A. OP Analysis

User outage is considered when the received SINRs fail to meet the rate-induced thresholds. With target rates r_c and r_k for the common and private streams, the corresponding thresholds are $\gamma_c^\dagger = 2^{r_c} - 1$ and $\gamma_k^\dagger = 2^{r_k} - 1$, respectively [21]. From (7), U_k has OP as

$$\begin{aligned} P_k^{\text{out}} &= 1 - \Pr\left[\gamma_c^k > \gamma_c^\dagger, \gamma_p^k > \gamma_k^\dagger\right] \\ &= 1 - \Pr\left[h_k^2 \geq \frac{\gamma_c^\dagger}{\alpha_c\beta_k - \gamma_c^\dagger\alpha_k\beta_k}, h_k^2 \geq \frac{\gamma_k^\dagger}{\alpha_k\beta_k - \gamma_k^\dagger\alpha_c\beta_k}\right] \\ &= \Pr\left[h_k^2 \leq \max\left\{\frac{\gamma_c^\dagger}{\alpha_c\beta_k - \gamma_c^\dagger\alpha_k\beta_k}, \frac{\gamma_k^\dagger}{\alpha_k\beta_k - \gamma_k^\dagger\alpha_c\beta_k}\right\}\right] \end{aligned} \tag{13}$$

where $\Pr[X, Y] \triangleq \Pr(X \cap Y)$ denotes the joint probability. After some steps, we can have $P_k^{\text{out}} = F_{h_k^2}(\theta_k)$, where $\theta_k = \min(\max\{(\gamma_c^\dagger)/((\alpha_c - \gamma_c^\dagger\alpha_k)\beta_k), (\gamma_k^\dagger)/((\alpha_k - \gamma_k^\dagger\alpha_c)\beta_k), \xi_{\min}\}, \xi_{\max})$. Furthermore, to make $P_k^{\text{out}} < 1$, we should have β_k satisfy $\alpha_c > \gamma_c^\dagger\alpha_k$ and $\alpha_k > \gamma_k^\dagger\alpha_c$.

Proposition 1: For the special case, when transmitting a common message on all the private channels, the achievable rate of the private part will decrease since it is now used to transmit both common and private data. The OP can be written as

$$\begin{aligned} &P_k^{\text{out}} \\ &= 1 - \Pr\left[\frac{(\alpha_c + \alpha_k)\beta_k h_k^2}{\alpha_k\beta_k h_k^2 + 1} > \gamma_c^\dagger, \frac{\alpha_k\beta_k h_k^2}{(\alpha_c + \alpha_k)\beta_k h_k^2 + 1} > \gamma_k^\dagger\right] \\ &= F_{h_k^2}\left(\min\left\{\max\left(\frac{\gamma_c^\dagger}{\ell_c}, \frac{\gamma_k^\dagger}{\ell_k}, \xi_{\min}\right), \xi_{\max}\right\}\right) \end{aligned} \tag{14}$$

where $\ell_c = (\alpha_c + \alpha_k)\beta_k - \gamma_c^\dagger\alpha_k\beta_k$ and $\ell_k = \alpha_k\beta_k - \gamma_k^\dagger(\alpha_c + \alpha_k)\beta_k$.

B. Coverage Probability Analysis

Following prior work [20], the system coverage probability is defined as the probability that all of the users in the system can achieve reliable detection, which is given by

$$P^{\text{cov}} = \prod_{k=1}^{K}\left(1 - P_k^{\text{out}}\right) \tag{15}$$

Authorized licensed use limited to: Technical University of Ostrava. Downloaded on March 03,2026 at 20:56:13 UTC from IEEE Xplore. Restrictions apply.

assuming that the outage event at each user is independent. Moreover, we have P^{cov} is strictly decreasing in each individual OP P_k^{out}. The system is covered only if every user is not in an outage. Hence,

$$P^{\text{cov}} \le \min_{1\le k\le K}\left(1-P_k^{\text{out}}\right) = 1-\max_{1\le k\le K} P_k^{\text{out}}. \tag{16}$$

For a lower bound, apply the union bound to the union of outage events, which gives

$$1-P^{\text{cov}} \le \sum_{k=1}^{K} P_k^{\text{out}} \Rightarrow P^{\text{cov}} \ge 1-\sum_{k=1}^{K} P_k^{\text{out}}. \tag{17}$$

Combining (16) and (17) yields two-sided bounds.

Remark 1: The system coverage probability is jointly determined by the individual outage probabilities of all users. The upper bound implies that overall performance is dominated by the user with the worst channel condition. Consequently, the coverage probability exhibits a bottleneck behavior, highlighting the necessity of balanced power allocation strategies and interference management schemes. Moreover, the lower bound quantifies an additive penalty from all users, in which every increment in any P_k^{out} reduces a guaranteed floor on P^{cov} by the same amount. This bound is tight when outage events are nearly disjoint, and ensuring $\sum_{k=1}^{K} P_k^{\text{out}} \le 1-\varepsilon$ would guarantee $P^{\text{cov}} \ge \varepsilon$.

C. Ergodic Sum Rate Analysis

The ergodic sum rate of RSMA can be given at the next page, where $\xi_0 = (1)/(r_e^2)(1)/(m+3)(C(m+1)L^{m+1})^{(2)/(m+3)}$, $A_1 = \alpha_k\beta_k + \alpha_c\beta_k, A_2 = \alpha_k\beta_k$, $A_3 = \alpha_c\beta_k + \alpha_k\beta_k$, $A_4 = \alpha_c\beta_k$, and $\omega = -(1)/(m+3) - 1$. Also, we have

$$\Upsilon(t,\varpi,\vartheta) = \frac{\log_2(\varpi t+1)\cdot t^{1-\vartheta}}{2(1-\vartheta)} + \frac{1}{2\ln 2}\frac{\varpi t^{2-\vartheta}\,{}_2F_1\left[1,2-\vartheta,3-\vartheta,-\varpi t\right]}{(-2+\vartheta)(1-\vartheta)} \tag{18}$$

with hypergeometric function ${}_2F_1$. A complete proof is provided in the Appendix

$$\begin{aligned} R^{\text{sum}} = {} & \xi_0 \min_k \{\Upsilon(\xi_{\max}, A_1, -\omega) - \Upsilon(\xi_{\min}, A_1, -\omega) \\ & - \Upsilon(\xi_{\max}, A_2, -\omega) + \Upsilon(\xi_{\min}, A_2, -\omega)\} \\ & + \xi_0 \sum_{k=1}^{K} \Upsilon(\xi_{\max}, A_3, -\omega) - \Upsilon(\xi_{\min}, A_3, -\omega) \\ & - \Upsilon(\xi_{\max}, A_4, -\omega) + \Upsilon(\xi_{\min}, A_4, -\omega). \end{aligned} \tag{19}$$

Remark 2: From (19), the ergodic sum rate increases with larger power-splitting coefficients α_c, α_k, and β_k due to enhanced signal contributions, while it decreases with larger m or longer distance r_e to highlight the nonlinear impact of channel and allocation parameters on system performance.

D. Optimal Power Allocation

Next, we aim to provide a fair allocation of private powers by minimizing the worst case user outage, which can be defined as the following optimization problem:

$$\min_{\alpha_k} \max_k \; P_k^{\text{out}} \tag{P0}$$

$$\text{s.t.} \sum_{k=1}^{K} \alpha_k \le 1-\alpha_c, \quad \alpha_k \ge 0 \tag{20a}$$

where the constraint ensures that total allocated resources do not exceed available transmission power. We put $\alpha_c - \gamma_c^{\dagger}\alpha_k \ge 0$ and $\alpha_k - \gamma_k^{\dagger}\alpha_c \ge 0$ as sign constraints to ensure feasibility. Also, $F_{h_k^2}(\cdot)$ is increasing and we have equivalent problem as

$$\min_{\alpha_k,\theta_k} \max_k \; \theta_k \tag{P1}$$

$$\text{s.t.} \; \frac{1}{\beta_k}\max\left\{\frac{\gamma_c^{\dagger}}{\alpha_c-\gamma_c^{\dagger}\alpha_k}, \frac{\gamma_k^{\dagger}}{\alpha_k-\gamma_k^{\dagger}\alpha_c}\right\} \le \theta_k \tag{21a}$$

$$\xi_{\min} \le \theta_k \le \xi_{\max} \tag{21b}$$

$$\alpha_c - \gamma_c^{\dagger}\alpha_k \ge 0, \quad \alpha_k - \gamma_k^{\dagger}\alpha_c \ge 0 \tag{21c}$$

$$\sum_{k=1}^{K} \alpha_k \le 1-\alpha_c, \quad \alpha_k \ge 0. \tag{21d}$$

Let $s_k = 1/\theta_k$ and rewritten (21a)–(21b), (P1) becomes

$$\min_{\alpha_k,s_k} \max_k \; \frac{1}{s_k} \tag{P2}$$

$$\text{s.t.} \; \gamma_c^{\dagger} \le \beta_k(\alpha_c - \gamma_c^{\dagger}\alpha_k)\, s_k \tag{22a}$$

$$\gamma_k^{\dagger} \le \beta_k(\alpha_k - \gamma_k^{\dagger}\alpha_c)\, s_k \tag{22b}$$

$$\frac{1}{\xi_{\max}} \le s_k \le \frac{1}{\xi_{\min}}, \tag{22c}$$

$$\alpha_c - \gamma_c^{\dagger}\alpha_k \ge 0, \quad \alpha_k - \gamma_k^{\dagger}\alpha_c \ge 0 \tag{22d}$$

$$\sum_{k=1}^{K} \alpha_k \le 1-\alpha_c, \quad \alpha_k \ge 0. \tag{22e}$$

Since the objective function is nonconvex in s_k, we consider $z_k = \ln s_k$ so that $1/s_k = e^{-z_k}$. We now combine the inequalities in (22a)–(22b) with (22c), and introduce an epigraph variable t to represent the maximum. This leads to

$$\min_{\alpha_k,z_k,t} \; t \tag{P3}$$

$$\text{s.t.} \; \gamma_c^{\dagger} e^{z_k} \le \beta_k\left(\alpha_c - \gamma_c^{\dagger}\alpha_k\right) \tag{23a}$$

$$\gamma_k^{\dagger} e^{z_k} \le \beta_k\left(\alpha_k - \gamma_k^{\dagger}\alpha_c\right) \tag{23b}$$

$$\alpha_c - \gamma_c^{\dagger}\alpha_k \ge 0, \quad \alpha_k - \gamma_k^{\dagger}\alpha_c \ge 0 \tag{23c}$$

$$\ln\left(1/\xi_{\max}\right) \le z_k \le \ln\left(1/\xi_{\min}\right) \tag{23d}$$

$$\sum_{k=1}^{K} \alpha_k \le 1-\alpha_c, \quad \alpha_k \ge 0 \tag{23e}$$

$$e^{-z_k} \le t. \tag{23f}$$

It can be seen that the objective in (P3) is linear. The power and nonnegativity constraints in (23e), the sign constraints in (23c), and the constraints on z_k in (23d) are affine. Moreover, the constraints (23a)–(23b) can be written in the disciplined convex programming (DCP) form with a nonnegative right side ensured by (23c) while the constraint (23f) is also exponential-cone representable. Consequently, (P3) can be efficiently solved by solvers such as CVX [22]. The offline power-allocation problem (P3) is an exponential-cone program with $2K+1$ variables and $8K+1$ constraints. A standard interior-point method requires $O(K^3)$ arithmetic per iteration and a small number of iterations to achieve acceptable convergence tolerance in practice.

Authorized licensed use limited to: Technical University of Ostrava. Downloaded on March 03,2026 at 20:56:13 UTC from IEEE Xplore. Restrictions apply.

TABLE I
SIMULATION PARAMETERS

Notation	Description	Value
α_c	Common power coeff.	-
α_k	Private power coeffs.	-
r_c	Common rate (bpcu)	0.3
r_k	Private rates (bpcu)	$(0.2, 0.3, 0.5)$
m	Lambertian order	1 (from $\Phi_{1/2} = 60°$)
L	LED height (m)	2.15
r_e	Cell radius (m)	3
A_k	PD area (m^2)	1×10^{-4}
Q_k	PD responsivity (A/W)	0.4
$U(\psi_k)$	Filter gain	1
$g(\psi_k)$	Concentrator gain	1
$\Phi_{1/2}$	LED semi-angle (deg)	60
Ψ_{fov}	PD FOV (deg)	60
n	Refractive index	1

IV. NUMERICAL RESULTS

In this section, we validate the analytical framework developed in Section III through Monte Carlo simulations to obtain thoughtful insights into the performance of RSMA in multicolor VLC systems. All simulations use the baseline settings in Table I for consistency and reproducibility.

We consider the case where the transmitter employs four LEDs of different colors, with the cross-talk matrix as

$$\mathbf{V} = \begin{bmatrix} 0.82 & 0 & 0 & 0 \\ 0.18 & 0.91 & 0 & 0 \\ 0 & 0.09 & 0.78 & 0 \\ 0 & 0 & 0.22 & 1 \end{bmatrix} \tag{24}$$

which characterizes the wavelength-dependent channel mixing among the color components. Note that small random perturbations of $\mathbf{V}$ do not alter the performance trends and only cause modest shifts of the curves.

Throughout this section, the proposed RSMA scheme is compared against conventional techniques such as NOMA and OMA for multicolor-LED. For fairness under equal resource sharing and transmit SNR, we divide the RSMA common rate evenly into the baseline targets. For white-LED RSMA comparison, we adapt the proposed scheme in [16] as a not strictly fair comparison since multicolor incurs cross-color coupling and per-color bias constraints absent in the white-LED case. We begin to examine the impact of the common power allocation coefficient α_c on the system coverage probability. In particular, both two-user and three-user scenarios are considered with multicolor LEDs at the transmitter side.

Fig. 2 shows the coverage probability of the proposed two-users RSMA-VLC system as a function of the average SNR for different values of the common power factor α_c and equal private power factors. The analytical and simulation curves are matched, which validates the accuracy of our derivations. It can be observed that when α_c has a relatively low value, such as $\alpha_c = 0.1$, almost all power is assigned to private streams, leading to the undecodable common stream. As a result, the coverage probability remains nearly zero across the entire SNR range. Similarly, when α_c is excessively high, such as $\alpha_c = 0.8$, most of the power is allocated to the common stream while the private parts receive insufficient power, again

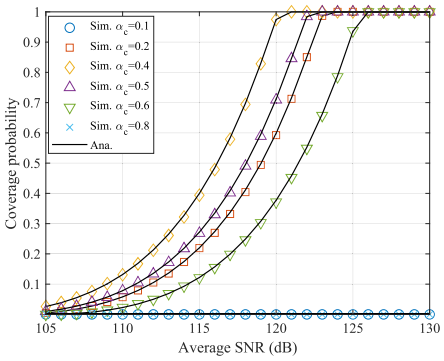

Fig. 2. Coverage probability versus average SNR for different common power allocation factors α_c.

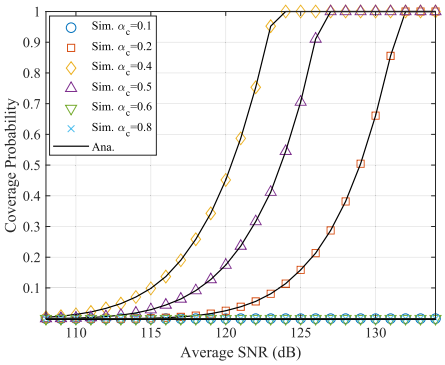

Fig. 3. Coverage probability for $K = 3$ users with $L = 4$ multicolor LEDs under different α_c values.

leading to a coverage probability close to zero for all SNRs. In contrast, for moderate values such as $\alpha_c \in [0.4, 0.6]$, the coverage probability rapidly increases with SNR and reaches unity at acceptable ranges. This indicates that an optimal range of α_c exists, where a balance between the common and private streams maximizes system coverage probability.

Similarly, Fig. 3 illustrates the system coverage probability for a VLC system employing three users and a four-color LED transmitter. The derived analytical results align well with the corresponding simulation data. Furthermore, the coverage probability approaches zero across the entire SNR range when the component correlation coefficient ρ_c is set to extreme values, such as 0.1 or 0.8, similar to the preceding analysis. For moderate values of α_c, the system performance improves significantly. In particular, when $\alpha_c = 0.4$ or $\alpha_c = 0.5$, the coverage probability increases sharply and approaches one at practical SNR values. This demonstrates that balancing the power between the common and private streams is essential to maximizing system reliability. With $\alpha_c = 0.2$ or $\alpha_c = 0.6$, the system still achieves full coverage but requires a higher SNR. The result insists on the importance of carefully designing power allocation strategies in RSMA-VLC systems with multiple users and multicolor LEDs.

Next, the system coverage probability versus the common power allocation coefficient α_c for a two-user VLC scenario under different SNR conditions is shown in Fig. 4. Similar to previous cases, for very low or very high values of α_c, the coverage probability degrades to nearly zero across all SNRs

Authorized licensed use limited to: Technical University of Ostrava. Downloaded on March 03,2026 at 20:56:13 UTC from IEEE Xplore. Restrictions apply.

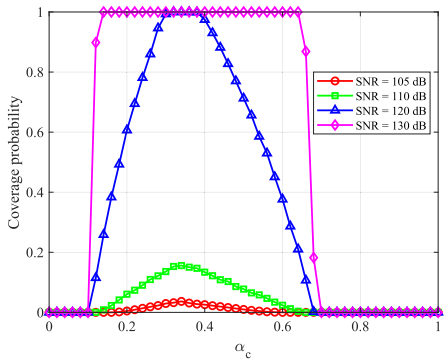

Fig. 4. Coverage probability versus α_c for a two-user VLC system under different SNR values.

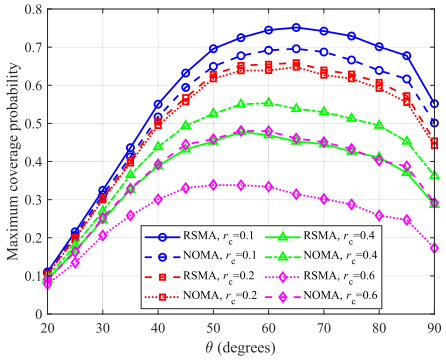

Fig. 6. Maximum coverage probability versus LED semiangle θ for two users under different r_c.

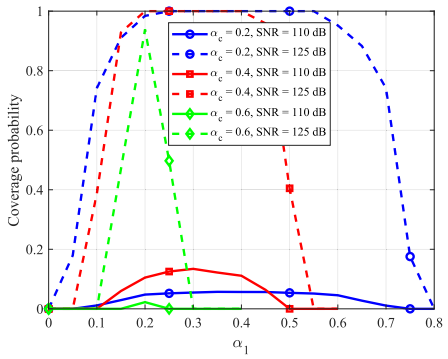

Fig. 5. Coverage probability versus α_1 for a two-user VLC system under different α_c and SNR values.

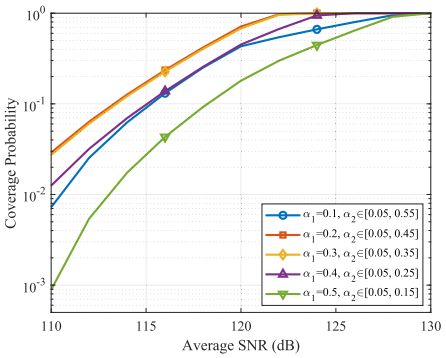

Fig. 7. Coverage probability versus average SNR with fixed $\alpha_c = 0.3$ and varying α_1.

due to the inability to decode. When α_c is chosen within a moderate range, the system achieves significantly better performance. For example, at α_c around 0.4–0.6, the coverage probability increases rapidly with SNR. At lower SNR values such as 105 and 110 dB, the maximum achievable coverage probability is much smaller, and the system is unable to support both users simultaneously with high reliability, regardless of how the power is allocated. These results confirm that the optimal region broadens as SNR increases, demonstrating the critical role of transmit power in RSMA-VLC system design.

In Fig. 5, we show the system coverage probability as a function of the private-power coefficient of U_1, α_1, for a two-user scenario where the common-power coefficient $\alpha_c \in \{0.2, 0.4, 0.6\}$. The results at SNR of 110 and 125 dB indicate a significant impact of both α_c and SNR value and reveal that coverage is maximized only within a finite interval of α_1. At moderate SNR, the coverage probability is relatively low, while increasing SNR to 125 dB substantially improves the feasible region. For example, with $\alpha_c = 0.6$, the feasible set reduces to a small neighborhood around the best point, and outside this range, the coverage rapidly goes to zero since the residual private power $1-\alpha_c$ is too small to satisfy both users' requirements simultaneously.

Fig. 6 shows the comparison of the maximum coverage probability as a function of the LED semiangle θ for a two-user VLC system using both RSMA and NOMA. For each θ and each common rate target $r_c \in \{0.1, 0.2, 0.4, 0.6\}$, the power-allocation variables are optimized to maximize the coverage probability, where the same rate constraints are imposed on RSMA and NOMA for a fair comparison. First, RSMA consistently outperforms NOMA over the entire θ range for r_c at low values, where interference management and power-splitting flexibility are most beneficial. Second, for any fixed value of r_c, the coverage probability increases as θ grows from 20° and peaks around 55° to 60°, then gradually decreases toward 90°. This trend reflects the tradeoff between improved coverage area at moderate θ and increased path loss.

Fig. 7 illustrates the maximum coverage probability as a function of the average SNR for a three-user system with a fixed common power allocation $\alpha_c = 0.3$. Six different curves correspond to allocations of private power for U_1, $\alpha_1 \in \{0.1, 0.2, 0.3, 0.4, 0.5, 0.6\}$, while the power of U_2, α_2 is varied to find the optimal value, and the remainder is allocated to the third user. As expected, the coverage probability improves monotonically with increasing SNR, approaching unity in the high-SNR regime regardless of the power allocation. Moreover, moderate allocations of $\alpha_1 = 0.2$ or $\alpha_1 = 0.3$ consistently achieve superior coverage, outperforming both highly unbalanced allocations of $\alpha_1 = 0.1$ and $\alpha_1 \geq 0.4$. This observation indicates that excessively favoring one user's private stream degrades fairness, leading to a lowering the overall coverage. Furthermore, the gap between curves diminishes as the SNR grows large, confirming that power allocation is more critical in the interference-limited regime, but even suboptimal splits can achieve near-perfect reliability in the high SNR range. This demonstrates that carefully tuning α_1 within a moderate

Authorized licensed use limited to: Technical University of Ostrava. Downloaded on March 03,2026 at 20:56:13 UTC from IEEE Xplore. Restrictions apply.

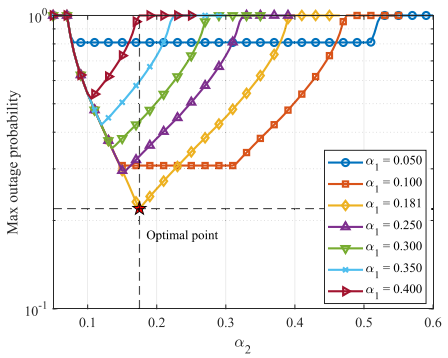

Fig. 8. Maximum OP versus α_2 for different values of α_1 with fixed $\alpha_c = 0.3$ in a three-user system.

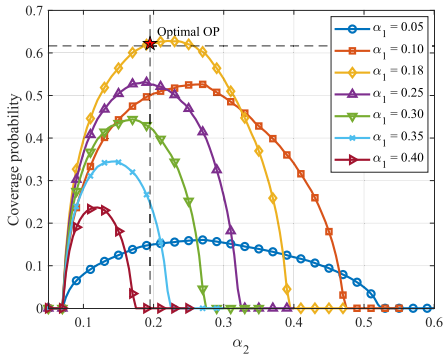

Fig. 9. Coverage probability versus α_2 at SNR = 120 dB with $\alpha_c = 0.3$ and fixed α_1.

range enhances system robustness compared with either highly asymmetric or overly uniform distributions.

In Fig. 8, we plot the maximum OP of the three-user RSMA-VLC system as a function of the private-power coefficient α_2 for different values of α_1, while the common power coefficient is fixed at $\alpha_c = 0.3$. It can be observed that the system performance is highly sensitive to the choice of private power allocation. For both very small and very large values of α_1, the worst-user OP remains close to one. The curves shown a minimum point for values at $\alpha_1 = 0.181$ and $\alpha_2 = 0.175$ that can also be determined by solving optimization problem (P3), confirming the existence of an optimal allocation that minimizes the maximum user outage. The optimal point is highlighted in the figure, at which the worst-user OP drops below 0.2. The results confirm that the RSMA strategy with optimized power allocation provides robustness against user imbalance and achieves more reliable communication in multicolor VLC systems with multiple users.

Fig. 9 presents the coverage probability when varying the power-allocation parameter α_2 for fixed α_c and α_1 with SNR = 120 dB. We can see that an increasing α_2 improves the performance of U_2 but simultaneously reduces the power for the other streams, thereby shifting the system degradation to the remaining users. We also show the optimal allocation for (P3) at $\alpha_1 = 0.195$. It can be observed that the maximum coverage probability occurs with the same value of α_1 but slightly different values of α_2 and α_3. This indicates that optimal power allocation for optimal OP can still significantly improve the

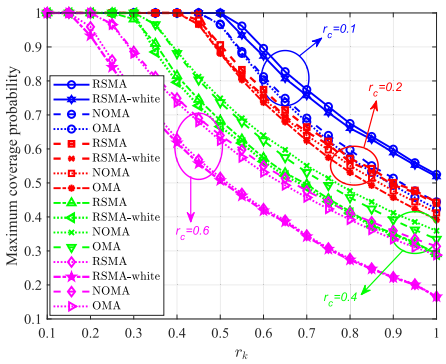

Fig. 10. Maximum coverage probability comparison of various schemes at SNR = 115 dB.

coverage performance even though it is not the global optimal one. Across α_1, moderate allocations $\alpha_1 \in [0.18, 0.30]$ provide remarkably higher peaks. When α_1 is too small, U_1 becomes the bottleneck and negatively impacts the coverage. When α_1 is too large, the feasible set of α_2 shrinks and either U_2 or U_3 becomes worse, significantly reduce P_{cov}.

Fig. 10 presents the maximum coverage probability with different values of the private target rate r_k for a two-user VLC system where the overall target rate of the two users is equal. For each value of r_k and each common-rate target $r_c \in \{0.1, 0.2, 0.4, 0.6\}$, the power allocation is adjusted to maximize the coverage. As can be observed, for any value of r_c, the maximum coverage probability decreases monotonically as r_k increases. On the other hand, RSMA outperforms NOMA across the whole range of r_k for small values of r_c but performs worse when the value of r_c increases.

Fig. 10 presents the maximum coverage probability versus the private-rate target r_k for $r_c \in \{0.1, 0.2, 0.4, 0.6\}$ under the two-user case, where power allocation is optimized at each point. For any r_c, the maximum coverage decreases monotonically with increasing r_k. At low common-rate targets, RSMA with multicolor LEDs achieves the highest coverage across the entire r_k range, followed by RSMA with white LEDs, NOMA, and OMA. As r_c grows, the RSMA advantage narrows and NOMA becomes the best one at larger r_k, while OMA remains the weaker baseline. These results highlight the critical role of the common-rate target, that allocating an appropriate r_c ratio is necessary for RSMA, especially in the multicolor configuration, to deliver the highest coverage gains.

Fig. 11 illustrates the maximum sum rate performance versus SNR for a two-user VLC system when varying the LED semiangle $\theta \in \{10°, 30°, 50°, 70°\}$. More specifically, when $\theta = 10°$, the narrow semiangle leads to the lowest channel coverage and very low sum rate. In this case, both RSMA and NOMA achieve only modest gains even at high SNR. In contrast, larger semiangles such as $\theta = 30°, 50°, 70°$ significantly improve the achievable sum rate, as the channel overlap improves multiuser signal strength. On the other hand, RSMA consistently outperforms NOMA across all considered θ values, while increasing θ above a certain value does not indefinitely improve performance.

Authorized licensed use limited to: Technical University of Ostrava. Downloaded on March 03,2026 at 20:56:13 UTC from IEEE Xplore. Restrictions apply.

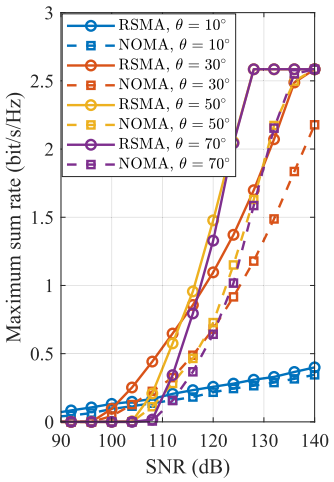

Fig. 11. Maximum sum rate versus LED semiangles θ.

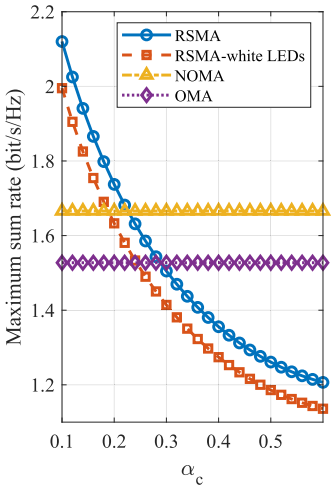

Fig. 12. Maximum sum rate versus α_c.

In Fig. 12, the maximum sum rate is shown versus the common-power coefficient α_c at SNR of 115 dB. For RSMA, the sum rate decreases with α_c, achieving the highest value at a small α_c where it clearly outperforms NOMA and OMA. Also, the white-LED RSMA performance has the same trend but remains slightly lower due to the absence of color-mixing gains. As α_c grows, RSMA loses its advantage near $\alpha_c = 0.23$, which indicates that allocating excessive power to the common stream degrades the sum-rate and that the multicolor benefit mostly in the low α_c regime.

V. Conclusion

This article proposed an analytical framework for evaluating the performance of RSMA in downlink multicolor VLC systems. More specifically, OP, ergodic sum rate, and coverage probability have been derived in closed form under realistic assumptions. Also, optimal precoding and power allocation coefficients have been considered to mitigate multiuser interference while exploiting color diversity. Consequently, analytical expressions have been validated by numerical simulations, which demonstrate a close match between simulation and analysis. Results show that proposed schemes significantly outperform conventional ones in terms of coverage probability and throughput for a low to moderate common rate. Moreover, it is revealed that an optimal range of common-power allocation exists while carefully optimizing power-splitting factors leads to robust system performance.

Appendix
Proof of (19)

We have the sum rate can be written as

$$\begin{aligned}
&R^{\text{sum}} \\
&= \min_k \mathbb{E}\left[R_c^k\right] + \sum_{k=1}^{K} \mathbb{E}\left[R_p^k\right] \\
&= \frac{1}{2}\int_{\xi_{\min}}^{\xi_{\max}} \left[\min_k \log_2\left(1+{\alpha_c}^k\right) + \sum_{k=1}^{K} \log_2\left(1+{\alpha_p}^k\right)\right] \\
&\quad \times f_{h_k^2}(t)\,dt \\
&= \xi_0 \underbrace{\min_k \int_{\xi_{\min}}^{\xi_{\max}} \frac{1}{2}\log_2\left(1+\frac{\alpha_c\beta_k t}{\alpha_k\beta_k t+1}\right) t^{-\frac{1}{m+3}-1}\,dt}_{I_1(t)} \\
&\quad + \xi_0 \underbrace{\sum_{k=1}^{K} \int_{\xi_{\min}}^{\xi_{\max}} \frac{1}{2}\log_2\left(1+\frac{\alpha_k\beta_k t}{\alpha_c\beta_k t+1}\right) t^{-\frac{1}{m+3}-1}\,dt}_{I_2(t)}. \qquad (25)
\end{aligned}$$

Consequently, $I_1(t)$ can be expressed as

$$\begin{aligned}
I_1(t) = \xi_0 \min_k \Bigg\{ &\underbrace{\int_{\xi_{\min}}^{\xi_{\max}} \frac{1}{2}\log_2\left(A_1 t+1\right) t^{-\omega} dt}_{I_3(t)} \\
&- \underbrace{\int_{\xi_{\min}}^{\xi_{\max}} \frac{1}{2}\log_2\left(A_2 t+1\right) t^{-\omega} dt}_{I_4(t)} \Bigg\}. \qquad (26)
\end{aligned}$$

After some manipulations, the first integral can be expressed as

$$\begin{aligned}
I_3(t) &= \frac{\log_2\left(A_1 t+1\right)\cdot t^{1-\omega}}{2\left(1-\omega\right)} - \frac{1}{2\ln 2}\frac{1}{1-\omega}\int \frac{A_1 t^{1-\omega}}{A_1 t+1} dt \\
&= \Upsilon\left(\xi_{\max}, A_1, -\omega\right) - \Upsilon\left(\xi_{\min}, A_1, -\omega\right). \qquad (27)
\end{aligned}$$

Consequently, we have

$$\begin{aligned}
I_1(t) = &\Upsilon\left(\xi_{\max}, A_1, -\omega\right) - \Upsilon\left(\xi_{\min}, A_1, -\omega\right) \\
&- \Upsilon\left(\xi_{\max}, A_2, -\omega\right) + \Upsilon\left(\xi_{\min}, A_2, -\omega\right). \qquad (28)
\end{aligned}$$

We then similarly obtain $I_2(t)$ and have the ergodic sum rate of proposed system as in (19).

References

[1] A. Al-Kinani, C.-X. Wang, L. Zhou, and W. Zhang, "Optical wireless communication channel measurements and models," *IEEE Commun. Surveys Tuts.*, vol. 20, no. 3, pp. 1939–1962, 3rd Quart., 2018.

[2] L. E. M. Matheus, A. B. Vieira, L. F. M. Vieira, M. A. M. Vieira, and O. Gnawali, "Visible light communication: Concepts, applications and challenges," *IEEE Commun. Surveys Tuts.*, vol. 21, no. 4, pp. 3204–3237, 4th Quart., 2019.

Authorized licensed use limited to: Technical University of Ostrava. Downloaded on March 03,2026 at 20:56:13 UTC from IEEE Xplore. Restrictions apply.

[3] T. Komine and M. Nakagawa, "Fundamental analysis for visible-light communication system using LED lights," *IEEE Trans. Consum. Electron.*, vol. 50, no. 1, pp. 100–107, Feb. 2004.

[4] M. Le Tran, S. Kim, T. Ketseoglou, and E. Ayanoglu, "LED selection and MAP detection for generalized LED index modulation," *IEEE Photon. Technol. Lett.*, vol. 30, no. 19, pp. 1695–1698, Oct. 15, 2018, doi: 10.1109/LPT.2018.2865591.

[5] A. Nuwanpriya, S.-W. Ho, and C. S. Chen, "Indoor MIMO visible light communications: Novel angle diversity receivers for mobile users," *IEEE J. Sel. Areas Commun.*, vol. 33, no. 9, pp. 1780–1792, Sep. 2015.

[6] M. Le-Tran and S. Kim, "Deep learning-based collaborative constellation design for visible light communication," *IEEE Commun. Lett.*, vol. 24, no. 11, pp. 2522–2526, Nov. 2020.

[7] A. Mishra, Y. Mao, O. Dizdar, and B. Clerckx, "Rate-splitting multiple access for 6G—Part I: Principles, applications and future works," *IEEE Commun. Lett.*, vol. 26, no. 10, pp. 2232–2236, Oct. 2022.

[8] M. Agiwal, A. Roy, and N. Saxena, "Next generation 5G wireless networks: A comprehensive survey," *IEEE Commun. Surveys Tuts.*, vol. 18, no. 3, pp. 1617–1655, 3rd Quart., 2016.

[9] R. C. Kizilirmak, C. R. Rowell, and M. Uysal, "Non-orthogonal multiple access (NOMA) for indoor visible light communications," in *Proc. 4th Int. Workshop Opt. Wireless Commun. (IWOW)*, Sep. 2015, pp. 98–101.

[10] S. A. H. Mohsan, M. Sadiq, Y. Li, A. V. Shvetsov, S. V. Shvetsova, and M. Shafiq, "NOMA-based VLC systems: A comprehensive review," *Sensors*, vol. 23, no. 6, p. 2960, Mar. 2023.

[11] Q. Liu, X. Xie, X. Wang, W. Wang, and L. Lu, "Rate splitting multiple access enhanced visible light communications under fairness constraint," in *Proc. 9th Int. Conf. Comput. Commun. (ICCC)*, Chengdu, China, Dec. 2023, pp. 125–130.

[12] Z. Qiu, Y. Mao, S. Ma, and B. Clerckx, "Robust max–min fair beamforming design for rate splitting multiple access-aided visible light communications," *IEEE Internet Things J.*, vol. 12, no. 8, pp. 10043–10057, Apr. 2025. [Online]. Available: https://ieeexplore.ieee.org/document/10772214

[13] L. Kong, W. Xu, H. Zhang, C. Zhao, and X. You, "R-OFDM for RGBA-LED-based visible light communication with illumination constraints," *J. Lightw. Technol.*, vol. 34, no. 23, pp. 5412–5422, Dec. 15, 2016.

[14] M. Le Tran and S. Kim, "Effective receiver design for MIMO visible light communication with quadrichromatic LEDs," *Electronics*, vol. 8, no. 12, p. 1383, Nov. 2019.

[15] B. G. Guzman and A. A. Dowhuszko, "Performance analysis of VLC systems with multi-color light sources beyond RGB LEDs," *J. Lightw. Technol.*, vol. 42, no. 16, pp. 5492–5505, Aug. 15, 2024.

[16] S. Naser et al., "Rate-splitting multiple access: Unifying NOMA and SDMA in MISO VLC channels," *IEEE Open J. Veh. Technol.*, vol. 1, pp. 393–413, 2020.

[17] K.-I. Ahn and J. K. Kwon, "Color intensity modulation for multicolored visible light communications," *IEEE Photon. Technol. Lett.*, vol. 24, no. 24, pp. 2254–2257, Dec. 15, 2012.

[18] Y. Yang et al., "Joint LED selection and precoding optimization for multiple-user multiple-cell VLC systems," *IEEE Internet Things J.*, vol. 9, no. 8, pp. 6003–6017, Apr. 2022.

[19] T.-H. Vu, Q. Pham, and S. Kim, "On performance of downlink THz-based rate-splitting multiple-access (RSMA): Is it always better than NOMA?," *IEEE Trans. Veh. Technol.*, vol. 73, no. 3, pp. 4435–4440, Mar. 2024.

[20] L. Yin, W. O. Popoola, X. Wu, and H. Haas, "Performance evaluation of non-orthogonal multiple access in visible light communication," *IEEE Trans. Commun.*, vol. 64, no. 12, pp. 5162–5175, Dec. 2016.

[21] S. T. Shah, K. W. Choi, T.-J. Lee, and M. Y. Chung, "Outage probability and throughput analysis of SWIPT enabled cognitive relay network with ambient backscatter," *IEEE Internet Things J.*, vol. 5, no. 4, pp. 3198–3208, Aug. 2018.

[22] (Sep. 2013). *CVX: MATLAB Software for Disciplined Convex Programming*. [Online]. Available: https://github.com/cvxr/CVX

Authorized licensed use limited to: Technical University of Ostrava. Downloaded on March 03,2026 at 20:56:13 UTC from IEEE Xplore. Restrictions apply.